Available online at www.sciencedirect.com
ScienceDirect
Composite Structures 82 (2008) 217–224
COMPOSITE STRUCTURES
cate/compstruct

Degradation investigation in a postbuckling composite stiffened fuselage panel

A.C. Orifici [a], R.S. Thomson [b,*], R. Degenhardt [c], A. Kling [c], K. Rohwer [c], J. Bayandor [d]

[a] School of Aerospace, Mechanical and Manufacturing Engineering, Royal Melbourne Institute of Technology, GPO Box 2476V, Melbourne, Vic. 3001, Australia
[b] Cooperative Research Centre for Advanced Composite Structures Limited, 506 Lorimer Street, Fishermans Bend, Vic. 3207, Australia
[c] Institute of Composite Structures and Adaptive Systems, DLR – German Aerospace Center, Lilienthalplatz 7, 38108 Braunschweig, Germany
[d] The Sir Lawrence Wackett Centre for Aerospace Design Technology, Royal Melbourne Institute of Technology, GPO Box 2476V, Melbourne, Vic. 3001, Australia

Available online 13 January 2007

COCOMAT is a four-year project under the European Commission 6th Framework Programme that aims to exploit the large strength reserves of composite structures through a more accurate prediction of collapse. Accordingly, one of the COCOMAT work packages involves the design of test panels with a focus on investigating the progression of composite damage mechanisms. This paper presents the collaborative results of some of the partners for this task. Different design alternatives were investigated for fuselage-representative test panels. Non-linear structural analyses were performed using MSC.Nastran and ABAQUS/Standard. Numerical predictions were also made applying a stress-based adhesive degradation model, previously implemented into a material user subroutine for ABAQUS/Standard. Following this, a fracture mechanics analysis using MSC.Nastran was performed along all interfaces between the skin and stiffeners, to examine the stiffener disbonding behaviour of each design. On the basis of the structural and fracture mechanics analyses, a design was selected as being the most suitable for the experimental investigation within COCOMAT. Though the COCOMAT panels have yet to be manufactured and tested, experimental data on the structural performance and damage mechanisms were available from a separate project for a panel identical to the selected design. This data was compared to the structural, degradation and fracture mechanics predictions made using non-linear finite element solutions, and the application of the design within the COCOMAT project was discussed.

: Composite; Buckling; Postbuckling; Stiffened panels; Skin–stiffener disbonding; COCOMAT

1. Introduction

The European Commission specific targeted research project ''Improved MATerial Exploitation at Safe Design of COmposite Airframe Structures by Accurate Simulation of COllapse'' (COCOMAT), is a currently running four- year project involving 15 international partners that aims to exploit the large strength reserves of postbuckling composite stiffened panels [1,2]. Currently, the onset of degradation in composite materials is not allowed, and composite structures must be designed with degradation occurring after the design ultimate load. The focus of COCOMAT is to produce a validated approach to include the effects of material degradation in the analysis, so that the final collapse of the structure can be more accurately predicted. This will allow composite structures to be designed with some degradation permitted, in a manner comparable to metallic structures where plasticity is already allowed between limit and ultimate loads. COCOMAT benefits from a high degree of synergy with the recently completed European Commission Framework Programme 5 project ''Improved POst-buckling SImulation for Design of Fibre COmposite Stiffened Fuselage

* Corresponding author. Fax: +61 3 9676 4900.
E-mail address: r. .au (R.S. Thomson).

0263-8223/$ - see front matter
pstruct.2007.01.012

Available online at www.sciencedirect.com
ScienceDirect
Composite Structures 82 (2008) 217–224
COMPOSITE STRUCTURES
cate/compstruct

Degradation investigation in a postbuckling composite stiffened fuselage panel

A.C. Orifici [a], R.S. Thomson [b,*], R. Degenhardt [c], A. Kling [c], K. Rohwer [c], J. Bayandor [d]

[a] School of Aerospace, Mechanical and Manufacturing Engineering, Royal Melbourne Institute of Technology, GPO Box 2476V, Melbourne, Vic. 3001, Australia
[b] Cooperative Research Centre for Advanced Composite Structures Limited, 506 Lorimer Street, Fishermans Bend, Vic. 3207, Australia
[c] Institute of Composite Structures and Adaptive Systems, DLR – German Aerospace Center, Lilienthalplatz 7, 38108 Braunschweig, Germany
[d] The Sir Lawrence Wackett Centre for Aerospace Design Technology, Royal Melbourne Institute of Technology, GPO Box 2476V, Melbourne, Vic. 3001, Australia

Available online 13 January 2007

COCOMAT is a four-year project under the European Commission 6th Framework Programme that aims to exploit the large strength reserves of composite structures through a more accurate prediction of collapse. Accordingly, one of the COCOMAT work packages involves the design of test panels with a focus on investigating the progression of composite damage mechanisms. This paper presents the collaborative results of some of the partners for this task. Different design alternatives were investigated for fuselage-representative test panels. Non-linear structural analyses were performed using MSC.Nastran and ABAQUS/Standard. Numerical predictions were also made applying a stress-based adhesive degradation model, previously implemented into a material user subroutine for ABAQUS/Standard. Following this, a fracture mechanics analysis using MSC.Nastran was performed along all interfaces between the skin and stiffeners, to examine the stiffener disbonding behaviour of each design. On the basis of the structural and fracture mechanics analyses, a design was selected as being the most suitable for the experimental investigation within COCOMAT. Though the COCOMAT panels have yet to be manufactured and tested, experimental data on the structural performance and damage mechanisms were available from a separate project for a panel identical to the selected design. This data was compared to the structural, degradation and fracture mechanics predictions made using non-linear finite element solutions, and the application of the design within the COCOMAT project was discussed.

: Composite; Buckling; Postbuckling; Stiffened panels; Skin–stiffener disbonding; COCOMAT

1. Introduction

The European Commission specific targeted research project "Improved **MAT**erial Exploitation at Safe Design of **CO**mposite Airframe Structures by Accurate Simulation of **CO**llapse" (COCOMAT), is a currently running four-year project involving 15 international partners that aims to exploit the large strength reserves of postbuckling composite stiffened panels [1,2]. Currently, the onset of degradation in composite materials is not allowed, and composite structures must be designed with degradation occurring after the design ultimate load. The focus of COCOMAT is to produce a validated approach to include the effects of material degradation in the analysis, so that the final collapse of the structure can be more accurately predicted. This will allow composite structures to be designed with some degradation permitted, in a manner comparable to metallic structures where plasticity is already allowed between limit and ultimate loads. COCOMAT benefits from a high degree of synergy with the recently completed European Commission Framework Programme 5 project "Improved **PO**st-buckling **SI**mulation for Design of Fibre **CO**mposite **S**tiffened Fuselage

* Corresponding author. Fax: +61 3 9676 4900.
E-mail address: r. .au (R.S. Thomson).

0263-8223/$ - see front matter © 2007 Elsevier Ltd. All rights reserved.
pstruct.2007.01.012

Structures'' (POSICOSS), which similarly investigated the behaviour of fuselage-representative stiffened composite panels in compression, but did not include the effects of material degradation.

One of the work packages of the COCOMAT project is the design of fuselage-representative panels for experimental testing. Within this work package, the German Aerospace Center (DLR) and the Cooperative Research Centre for Advanced Composite Structures (CRC-ACS) are collaborating to produce panel designs with a specific focus on the experimental investigation into skin–stringer disbonding. This paper outlines the results of the collaborative research work so far, which includes the selection of a design most appropriate for the investigation of skin–stringer disbonding based on structural and fracture mechanics analyses. Though COCOMAT panels have not yet been manufactured and tested, a comparison is made between the numerical predictions and experimental testing data for an identical panel from a separate project.

2. Panel design

2.1. Panel variations

Based on previous experience [3], a nominal panel was defined, and three variations were proposed. These variations, V12, V15 and V16 all used identical material and boundary conditions, though had slight variations in geometry in order to investigate the effect of the number of stiffeners and the height of the outer stiffeners, see Fig. 1 and Table 1. The V12 design used four stiffeners with the outside two made 6 mm (43%) taller and stiffer than the nominal design, whereas the V15 and V16 design both used the nominal stiffener size, but differed in using five and six stiffeners, respectively. Finite element (FE) models were generated for ABAQUS/Standard (Abaqus) and MSC.Nastran (Nas- tran), and are summarised in Table 2. The boundary condi- tions for all models were identical, with the axially loaded and fixed ends both fully clamped, and the resin-embedded

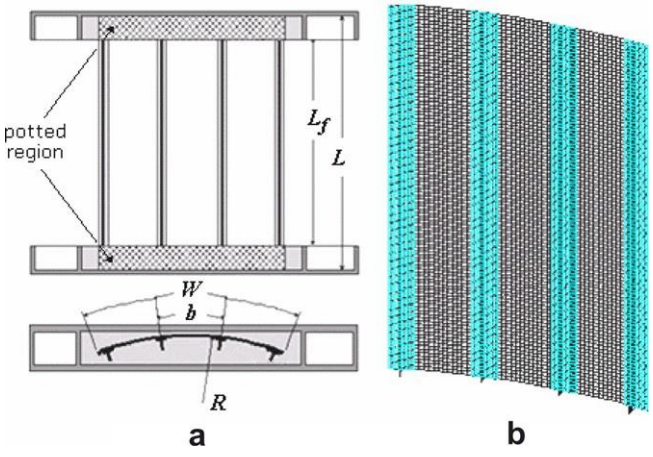

Fig. 1. Nominal panel design (a) geometry and (b) Abaqus FE model.

or ''potted'' region on both ends represented as an area in which only axial displacement was permitted, based on work by previous authors [3,4]. The main difference between the Abaqus and Nastran models was in the representation of the skin–stiffener interface, where the Nastran models used only rigid links to connect the elements in the skin and stiff- ener flange, while the Abaqus model used rigid links con- nected to a thin layer of solid elements between the skin and flange to represent an adhesive layer.

2.2. Analysis approach

The three panel variations were analysed with implicit solvers using a full Newton–Raphson procedure [5], where the default non-linear parameters of both software packages were used, except for a STABILIZE parameter of $2 \cdot 10^{-6}$ in Abaqus and a convergence tolerance level of ''Very High'' in Nastran. The STABILIZE parameter functions similar to a viscosity in Abaqus, where the addition of the factor reduces some of the energy of the panel to assist with convergence issues, and the ''Very High'' setting in Nastran corresponds to load and work residuals of $1 \cdot 10^{3}$ and $1 \cdot 10^{7}$, respectively. All panels were analysed to 4 mm axial compression, except for the Nastran V15 and V16 models, which only ran to 3.54 mm and 3.51 mm axial compression, respectively due to convergence problems.

For the Nastran models, use was made of a tool developed previously, Compdat [6], to calculate strain energy release rates (G) at all the skin–stiffener interfaces. The values of G in its modes I and II components were used in a mixed-mode failure law, given in Eq. (1), to determine the likelihood of skin–stiffener disbond initiation. In order to do this, values of G_{Ic} and G_{IIc} for the IM7/8552 material system were required, which were taken from Schön et al. [7,8], and are given in Table 3. The stiffeners in each panel were numbered starting from the topmost stiffener, as viewed in the XY plane, and skin–stiffener interfaces were designated as upper or lower for each stiffener in the same plane. The numbering system for all models is given in Fig. 2, where S is the stiffener number, I is the interface designation, and U and L are upper and lower, respectively. For each model, the sensitivity of the disbond predictions to the exponents of the mode I and II ratios m and n in Eq. (1), respectively) in the mixed-mode failure law was also investigated.

$$\left(\frac{G_I}{G_{Ic}}\right)^m + \left(\frac{G_{II}}{G_{IIc}}\right)^n = 1. \quad (1)$$

2.3. Analysis results

The load-shortening graphs for designs V12, V15 and V16 are given in Figs. 3–5, respectively. The agreement between Nastran and Abaqus results was very good, particularly for the local buckling. All designs were predicted to buckle into the same local buckling mode shape at an axial

Structures'' (POSICOSS), which similarly investigated the behaviour of fuselage-representative stiffened composite panels in compression, but did not include the effects of material degradation.

One of the work packages of the COCOMAT project is the design of fuselage-representative panels for experimental testing. Within this work package, the German Aerospace Center (DLR) and the Cooperative Research Centre for Advanced Composite Structures (CRC-ACS) are collaborating to produce panel designs with a specific focus on the experimental investigation into skin–stringer disbonding. This paper outlines the results of the collaborative research work so far, which includes the selection of a design most appropriate for the investigation of skin–stringer disbonding based on structural and fracture mechanics analyses. Though COCOMAT panels have not yet been manufactured and tested, a comparison is made between the numerical predictions and experimental testing data for an identical panel from a separate project.

2. Panel design

2.1. Panel variations

Based on previous experience [3], a nominal panel was defined, and three variations were proposed. These variations, V12, V15 and V16 all used identical material and boundary conditions, though had slight variations in geometry in order to investigate the effect of the number of stiffeners and the height of the outer stiffeners, see Fig. 1 and Table 1. The V12 design used four stiffeners with the outside two made 6 mm (43%) taller and stiffer than the nominal design, whereas the V15 and V16 design both used the nominal stiffener size, but differed in using five and six stiffeners, respectively. Finite element (FE) models were generated for ABAQUS/Standard (Abaqus) and MSC.Nastran (Nastran), and are summarised in Table 2. The boundary conditions for all models were identical, with the axially loaded and fixed ends both fully clamped, and the resin-embedded or ''potted'' region on both ends represented as an area in which only axial displacement was permitted, based on work by previous authors [3,4]. The main difference between the Abaqus and Nastran models was in the representation of the skin–stiffener interface, where the Nastran models used only rigid links to connect the elements in the skin and stiffener flange, while the Abaqus model used rigid links connected to a thin layer of solid elements between the skin and flange to represent an adhesive layer.

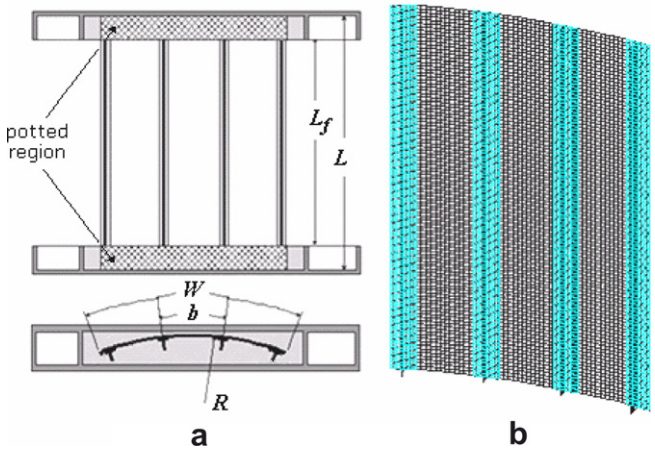

Fig. 1. Nominal panel design (a) geometry and (b) Abaqus FE model.

2.2. Analysis approach

The three panel variations were analysed with implicit solvers using a full Newton–Raphson procedure [5], where the default non-linear parameters of both software packages were used, except for a STABILIZE parameter of 2×10^{-6} in Abaqus and a convergence tolerance level of ''Very High'' in Nastran. The STABILIZE parameter functions similar to a viscosity in Abaqus, where the addition of the factor reduces some of the energy of the panel to assist with convergence issues, and the ''Very High'' setting in Nastran corresponds to load and work residuals of 1×10^{-3} and 1×10^{-7}, respectively. All panels were analysed to 4 mm axial compression, except for the Nastran V15 and V16 models, which only ran to 3.54 mm and 3.51 mm axial compression, respectively due to convergence problems.

For the Nastran models, use was made of a tool developed previously, Compdat [6], to calculate strain energy release rates (G) at all the skin–stiffener interfaces. The values of G in its modes I and II components were used in a mixed-mode failure law, given in Eq. (1), to determine the likelihood of skin–stiffener disbond initiation. In order to do this, values of G_{Ic} and G_{IIc} for the IM7/8552 material system were required, which were taken from Schön et al. [7,8], and are given in Table 3. The stiffeners in each panel were numbered starting from the topmost stiffener, as viewed in the XY plane, and skin–stiffener interfaces were designated as upper or lower for each stiffener in the same plane. The numbering system for all models is given in Fig. 2, where S is the stiffener number, I is the interface designation, and U and L are upper and lower, respectively. For each model, the sensitivity of the disbond predictions to the exponents of the mode I and II ratios m and n in Eq. (1), respectively) in the mixed-mode failure law was also investigated.

$$\left(\frac{G_I}{G_{Ic}}\right)^m+\left(\frac{G_{II}}{G_{IIc}}\right)^n\leqslant 1. \tag{1}$$

2.3. Analysis results

The load-shortening graphs for designs V12, V15 and V16 are given in Figs. 3–5, respectively. The agreement between Nastran and Abaqus results was very good, particularly for the local buckling. All designs were predicted to buckle into the same local buckling mode shape at an axial

Table 1
Panel parameters, all designs

Parameter	Panel design		
	V12	V15	V16
Panel length, L	780	780	780
Panel free length, L_f	660	660	660
Panel radius, R	1000	1000	1000
Stiffener pitch, b	129	129	129
Number of stiffeners	4 (2 inner, 2 outer)	5	6
Panel arc length, W	420	560	698
Material system	IM7/8552	IM7/8552	IM7/8552
Skin lay-up	$[90 \pm 45, 0]_S$	$[90 \pm 45, 0]_S$	$[90 \pm 45, 0]_S$
Stiffener height	inner: 14 outer: 20	14	14
Stiffener web lay-up	inner: $[(45, 45)_3, 0_6]_S$ outer: $[(45, 45)_3, 0_8]_S$	$[(45, 45)_3, 0_6]_S$	$[(45, 45)_3, 0_6]_S$
Ply thickness	0.125	0.125	0.125
Stiffener width	32	32	32

Table 2
FE model parameters, all designs

Number of elements	Abaqus			Nastran		
	V12	V15	V16	V12	V15	V16
Shells	19,968	25,584	31,200	28,860	24,804	30,264
Rigid bars	6280	7850	9420	7057	7066	8479
Solids	2496	3120	3744	–	–	–
Axial length	156		156		156	
Stiffener bay (between flanges)						
Stiffener height						
Stiffener flange						

Table 3
Fracture toughness values used, from literature

Property	Fracture toughness (J/m^2)	Reference
G_{Ic}	220	[7]
G_{IIc}	630	[8]

compression between 0.53 and 0.57 mm, which involved 15 longitudinal half sine waves per stiffener bay. The global buckling patterns of all panels were symmetrical, with all panels buckled inwards towards the centre of curvature. The V12 panel, with three stiffener bays, developed a single central global buckle at around 1.25 mm axial compression, whilst the V15 and V16 panels, with four and five stiffener bays, respectively, showed two global buckles in the outer stiffener bays developing at around 1 mm axial compression. Also, the V12 panel transitioned from local to global buckling via an anti-symmetric mode, and both the V12 and V16 panels showed a change to a secondary global buckling shape.

The results for failure prediction based on SERR and the mixed-mode failure criterion with two sets of power law exponents are summarised in Table 4, where failure is used here to mean the onset of skin–stringer disbonding, and not the final structural collapse of the panel. Failure was predicted to initiate at the edge stiffeners in design V12 and at the centre stiffeners for V15 and V16. The axial compression values for failure were very consistent across the three designs ranging from 1.39 to 1.44 mm for the indices $m = 1$ and $n = 1$. Changing the power law indices to

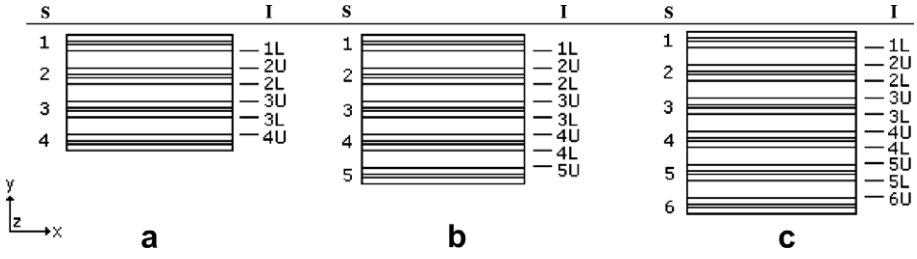

Fig. 2. skin–stiffener groups: (a) V12, (b) V15 and (c) V16.

Table 1
Panel parameters, all designs

Parameter	Panel design		
	V12	V15	V16
Panel length, L	780	780	780
Panel free length, L_f	660	660	660
Panel radius, R	1000	1000	1000
Stiffener pitch, b	129	129	129
Number of stiffeners	4 (2 inner, 2 outer)	5	6
Panel arc length, W	420	560	698
Material system	IM7/8552	IM7/8552	IM7/8552
Skin lay-up	$[90 \pm 45, 0]_S$	$[90 \pm 45, 0]_S$	$[90 \pm 45, 0]_S$
Stiffener height	inner: 14 outer: 20	14	14
Stiffener web lay-up	inner: $[(45,-45)_3, 0_6]_S$ outer: $[(45,-45)_3, 0_8]_S$	$[(45,-45)_3, 0_6]_S$	$[(45,-45)_3, 0_6]_S$
Ply thickness	0.125	0.125	0.125
Stiffener width	32	32	32

Table 2
FE model parameters, all designs

Number of elements	Abaqus			Nastran		
	V12	V15	V16	V12	V15	V16
Shells	19,968	25,584	31,200	28,860	24,804	30,264
Rigid bars	6280	7850	9420	7057	7066	8479
Solids	2496	3120	3744	–	–	–
Axial length	156	156	156	195	156	156
Stiffener bay (between flanges)	16	16	16	24	16	16
Stiffener height	4	4	4	3	3	3
Stiffener flange	8	8	8	8	8	8

Table 3
Fracture toughness values used, from literature

Property	Fracture toughness (J/m^2)	Reference
G_{Ic}	220	[7]
G_{IIc}	630	[8]

compression between 0.53 and 0.57 mm, which involved 15 longitudinal half sine waves per stiffener bay. The global buckling patterns of all panels were symmetrical, with all panels buckled inwards towards the centre of curvature. The V12 panel, with three stiffener bays, developed a single central global buckle at around 1.25 mm axial compression, whilst the V15 and V16 panels, with four and five stiffener bays, respectively, showed two global buckles in the outer stiffener bays developing at around 1 mm axial compression. Also, the V12 panel transitioned from local to global buckling via an anti-symmetric mode, and both the V12 and V16 panels showed a change to a secondary global buckling shape.

The results for failure prediction based on SERR and the mixed-mode failure criterion with two sets of power law exponents are summarised in Table 4, where failure is used here to mean the onset of skin–stringer disbonding, and not the final structural collapse of the panel. Failure was predicted to initiate at the edge stiffeners in design V12 and at the centre stiffeners for V15 and V16. The axial compression values for failure were very consistent across the three designs ranging from 1.39 to 1.44 mm for the indices $m = 1$ and $n = 1$. Changing the power law indices to

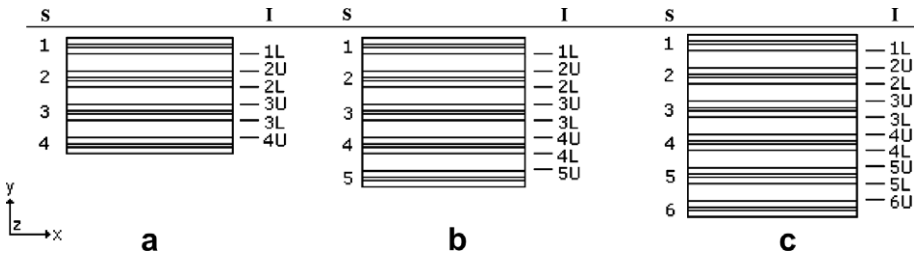

Fig. 2. skin–stiffener groups: (a) V12, (b) V15 and (c) V16.

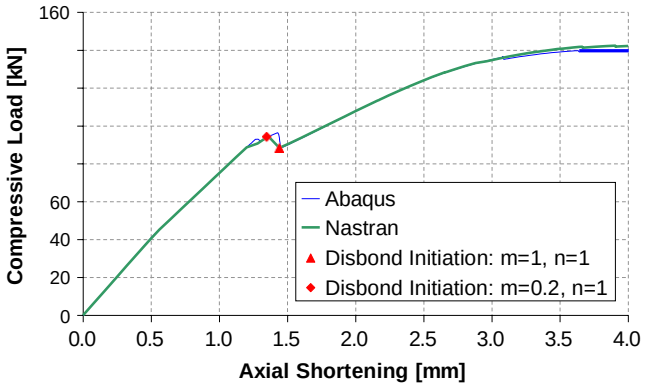

Fig. 3. V12 load-shortening, Abaqus and Nastran solutions.

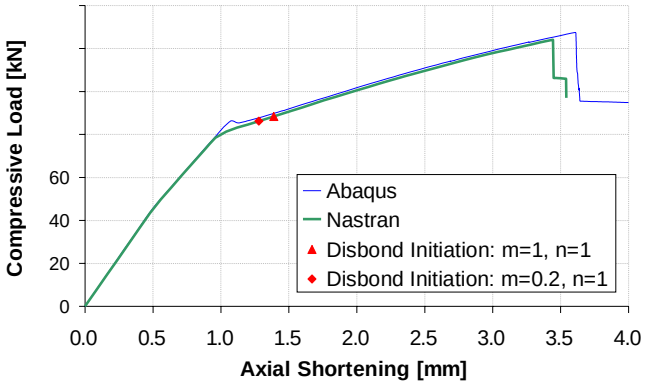

Fig. 4. V15 load-shortening, Abaqus and Nastran solutions.

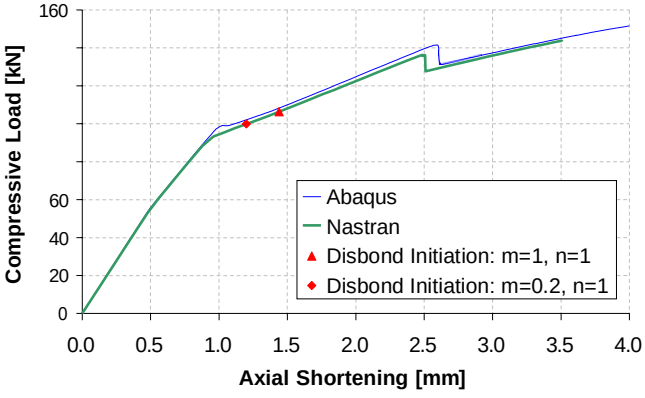

Fig. 5. V16 load-shortening, Abaqus and Nastran solutions.

m = 0.2 and n = 1 reduced the axial compression at failure by up to 17% for V16. In general, the predicted failure was Mode I dominated.

2.4. Design selection

As a result of the structural and fracture mechanics analyses on all proposed panels, panel design V15 was recommended as being best suited for experimental investigation of skin–stiffener disbonding. For this panel, the postbuckling behaviour was stable with a progressive change from local to a symmetric global buckling mode. The panel also exhibited a large stable global postbuckling zone from 0.96 to 3.45 mm axial compression, and stiffener disbonding was predicted to initiate clearly after global buckling. Finally, this panel showed the least sensitivity to the mixed-mode power law exponents for the predicted axial compression at failure initiation.

In contrast, the V12 panel analysis predicted that disbonding would initiate in the outer stiffeners first, which raised the possibility that disbond initiation could lead to catastrophic failure of the panel. Additionally, the progression from local to global buckling via an anti-symmetric global mode demonstrated less stable global buckling behaviour. Also, disbond initiation was predicted to coincide with the change from local to global buckling, which would make the accurate detection of initiation difficult during testing.

Separately, the V16 panel analysis predicted a reduced postbuckling zone as compared with the V15 panel, due to the secondary mode shape change occurring at 2.5 mm axial compression. This postbuckling mode shape change would not only be complicated by the existing skin–stiffener disbond, but would affect the investigation into disbond growth. The disbond initiation prediction for the V16 panel was also more sensitive to the power law exponents, which would make validation of degradation models more difficult.

3. Experimental testing

Though the COCOMAT test panels have yet to be manufactured and tested, experimental results were available as part of a separate DLR project on a panel identical to the selected design. These experimental results are summarised

Table 4
Predicted failure loads and locations

Panel	Power law exponents		Failure axial compression (mm)	Failure load (kN)	Stiffeners for failure	Lengthwise location (mm)	G_I/G_{II} at failure
V12	m = 1	n = 1	1.44	88	1L, 4U	472	1.6
	m = 0.2	n = 1	1.35	94	1L, 4U	472	1.6
V15	m = 1	n = 1	1.39	88	3U, 3L	390, 415	1.8
	m = 0.2	n = 1	1.28	86	3U, 3L	390, 415	1.8
V16	m = 1	n = 1	1.44	106	3U, 4L	465, 320	1.4
	m = 0.2	n = 1	1.20	100	3L	400	1.0

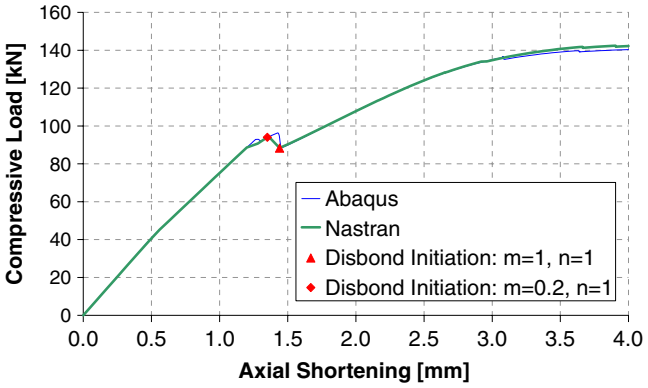

Fig. 3. V12 load-shortening, Abaqus and Nastran solutions.

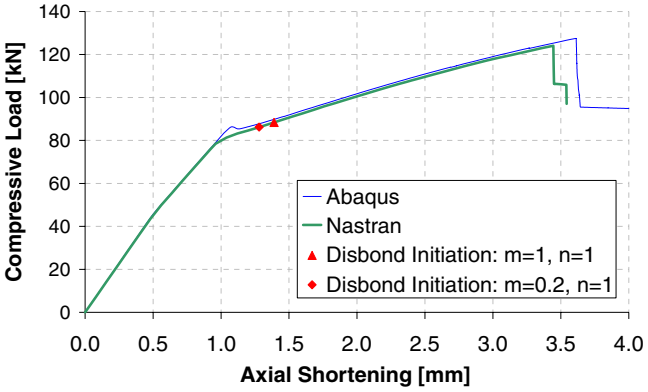

Fig. 4. V15 load-shortening, Abaqus and Nastran solutions.

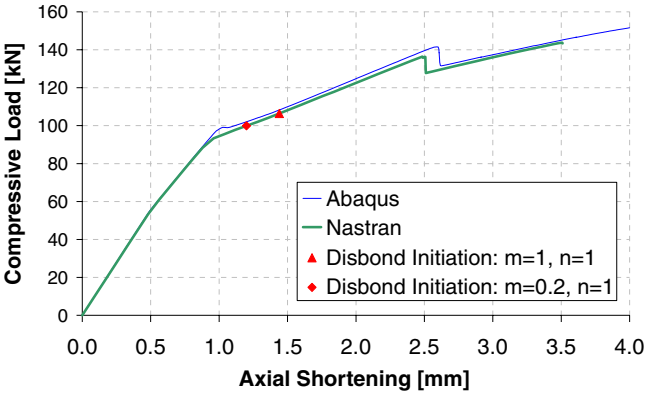

Fig. 5. V16 load-shortening, Abaqus and Nastran solutions.

$m = 0.2$ and $n = 1$ reduced the axial compression at failure by up to 17% for V16. In general, the predicted failure was Mode I dominated.

2.4. Design selection

As a result of the structural and fracture mechanics analyses on all proposed panels, panel design V15 was recommended as being best suited for experimental investigation of skin–stiffener disbonding. For this panel, the postbuckling behaviour was stable with a progressive change from local to a symmetric global buckling mode. The panel also exhibited a large stable global postbuckling zone from 0.96 to 3.45 mm axial compression, and stiffener disbonding was predicted to initiate clearly after global buckling. Finally, this panel showed the least sensitivity to the mixed-mode power law exponents for the predicted axial compression at failure initiation.

In contrast, the V12 panel analysis predicted that disbonding would initiate in the outer stiffeners first, which raised the possibility that disbond initiation could lead to catastrophic failure of the panel. Additionally, the progression from local to global buckling via an anti-symmetric global mode demonstrated less stable global buckling behaviour. Also, disbond initiation was predicted to coincide with the change from local to global buckling, which would make the accurate detection of initiation difficult during testing.

Separately, the V16 panel analysis predicted a reduced postbuckling zone as compared with the V15 panel, due to the secondary mode shape change occurring at 2.5 mm axial compression. This postbuckling mode shape change would not only be complicated by the existing skin–stiffener disbond, but would affect the investigation into disbond growth. The disbond initiation prediction for the V16 panel was also more sensitive to the power law exponents, which would make validation of degradation models more difficult.

3. Experimental testing

Though the COCOMAT test panels have yet to be manufactured and tested, experimental results were available as part of a separate DLR project on a panel identical to the selected design. These experimental results are summarised

Table 4
Predicted failure loads and locations

Panel	Power law exponents		Failure axial compression (mm)	Failure load (kN)	Stiffeners for failure	Lengthwise location (mm)	G_I/G_{II} at failure
V12	$m = 1$	$n = 1$	1.44	88	1L, 4U	472	1.6
	$m = 0.2$	$n = 1$	1.35	94	1L, 4U	472	1.6
V15	$m = 1$	$n = 1$	1.39	88	3U, 3L	390, 415	1.8
	$m = 0.2$	$n = 1$	1.28	86	3U, 3L	390, 415	1.8
V16	$m = 1$	$n = 1$	1.44	106	3U, 4L	465, 320	1.4
	$m = 0.2$	$n = 1$	1.20	100	3L	400	1.0

in Fig. 6 and in the first row of Fig. 9, which respectively show the load versus axial compression (load-shortening) values taken from between the loading platens, and deformation patterns obtained from photogrammetric measurement conducted. Note that where possible the figures of deformation patterns were taken just after points of mode shape change, and that all images face the stiffener side of the panel. The test procedure involved pre-test loadings to settle experimental non-linearities and calibrate the measuring equipment, then quasi-static loading until collapse. After the occurrence of global buckling, the loading was briefly stopped to inspect the panel and perform subse- quent measurements, the effect of which is seen in a slight reduction in the panel load at around 1.34 mm axial compression.

Under loading, the panel underwent local buckling of 15 longitudinal half sine waves per stiffener bay at an axial compression of 0.51 mm. This deformation pattern was slightly asymmetric, with one side of the panel moving towards and the other side moving away from the centre of curvature, where the outwards moving edge corresponds to stiffener 5 in Fig. 2b. First global buckling occurred at 74.4 kN or 0.97 mm compression, with an asymmetric deformation pattern of two global buckles in the outer stiffener bays consisting of the same inward and outward global buckles. A secondary global buckling shape developed at around 1.72 mm compression, where the inward global buckle grew to the adjacent inner stiffener bay. The collapse of the panel occurred at 83.6 kN or 2.71 mm axial compression, and was characterised by an extreme aural event, and a sharp reduction in the load-carrying capacity of the panel.

From visual inspection, the failed panel showed a variety of composite damage mechanisms, including fibre fracture in both the stiffener blade and flange, matrix cracking in the skin and stiffener blade and flange, and multiple delaminations in the region between the skin and stiffener and between ply groups in the stiffener blade, see Fig. 7. The collapse of the panel was likely due to fibre fracture across the blade in the centre of the stiffener 5, located at the edge of the outward global buckle. There were also regions of

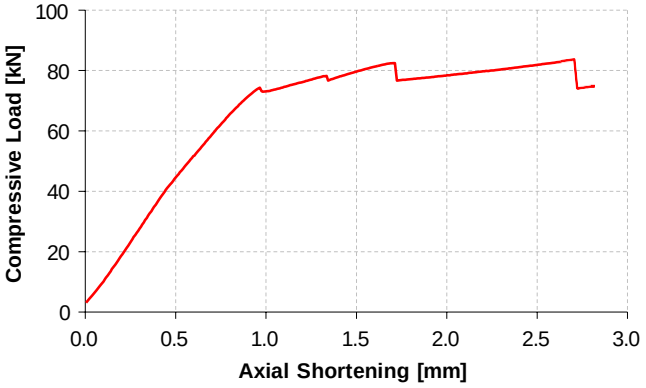

Fig. 6. Experimental load-shortening graph.

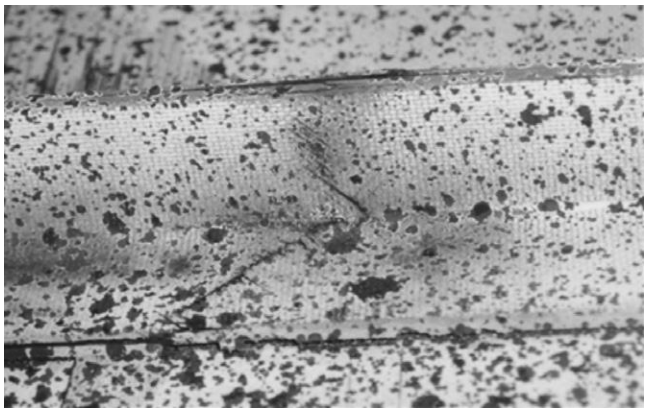

Fig. 7. Disbonded region in central stiffener, unloaded after collapse, showing composite damage mechanisms present from visual inspection throughout the panel: delamination, fibre fracture and matrix cracking in the stiffener blade, fibre fracture and matrix cracking in the stiffener flange, multiple delaminations between the skin and stiffener, and matrix cracking in the skin.

significant separation between the skin and stiffener where the stiffener buckled locally away from the skin, in both the centre of the middle stiffener (stiffener 3) and close to the potting in one of the inner stiffeners (stiffener 4) on the non-loading side.

4. Comparison of results

In addition to the design calculations, an FE model with geometric imperfections was created by applying panel imperfections from the photogrammetric measurement of the unloaded panel to the V15 Nastran model. As an additional numerical comparison, the V15 Abaqus model was also analysed with a degradation methodology previously developed and implemented using the Abaqus USDFLD material user subroutine [9]. The subroutine was applied to the elements of the adhesive between the skin and stiffener, and monitored maximum stress failure criteria coupled to corresponding stiffness reductions upon satisfaction of the criteria as a means of modelling degradation in the skin–stiffener interface. The strength properties of the adhesive were taken from manufacturer data sheets [10] and are summarised in Table 5. For the USDFLD, a value of 0.1% was used as the reduction for the stiffness properties, on the basis of a parametric study and on the assumption that a value as close to zero as numerically possible was required in order to simulate the loss of load-

Table 5
Redux 312 material properties, from literature

Property	
E_1 (MPa)	3000
ν_{12}	0.30
Maximum compressive stress (MPa)	48
Maximum shear stress (MPa)	38
Maximum normal stress (MPa)	8

in Fig. 6 and in the first row of Fig. 9, which respectively show the load versus axial compression (load-shortening) values taken from between the loading platens, and deformation patterns obtained from photogrammetric measurement conducted. Note that where possible the figures of deformation patterns were taken just after points of mode shape change, and that all images face the stiffener side of the panel. The test procedure involved pre-test loadings to settle experimental non-linearities and calibrate the measuring equipment, then quasi-static loading until collapse. After the occurrence of global buckling, the loading was briefly stopped to inspect the panel and perform subsequent measurements, the effect of which is seen in a slight reduction in the panel load at around 1.34 mm axial compression.

Under loading, the panel underwent local buckling of 15 longitudinal half sine waves per stiffener bay at an axial compression of 0.51 mm. This deformation pattern was slightly asymmetric, with one side of the panel moving towards and the other side moving away from the centre of curvature, where the outwards moving edge corresponds to stiffener 5 in Fig. 2b. First global buckling occurred at 74.4 kN or 0.97 mm compression, with an asymmetric deformation pattern of two global buckles in the outer stiffener bays consisting of the same inward and outward global buckles. A secondary global buckling shape developed at around 1.72 mm compression, where the inward global buckle grew to the adjacent inner stiffener bay. The collapse of the panel occurred at 83.6 kN or 2.71 mm axial compression, and was characterised by an extreme aural event, and a sharp reduction in the load-carrying capacity of the panel.

From visual inspection, the failed panel showed a variety of composite damage mechanisms, including fibre fracture in both the stiffener blade and flange, matrix cracking in the skin and stiffener blade and flange, and multiple delaminations in the region between the skin and stiffener and between ply groups in the stiffener blade, see Fig. 7. The collapse of the panel was likely due to fibre fracture across the blade in the centre of the stiffener 5, located at the edge of the outward global buckle. There were also regions of

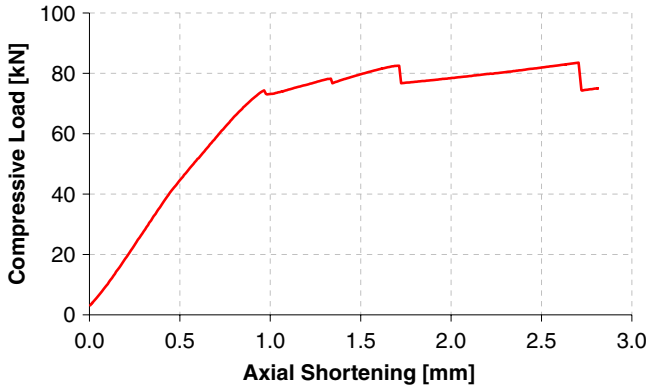

Fig. 6. Experimental load-shortening graph.

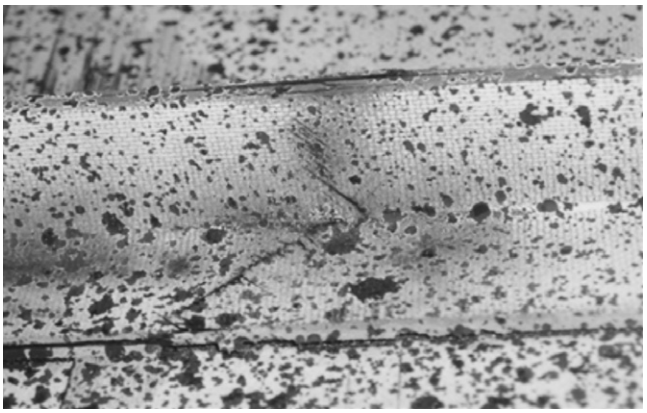

Fig. 7. Disbonded region in central stiffener, unloaded after collapse, showing composite damage mechanisms present from visual inspection throughout the panel: delamination, fibre fracture and matrix cracking in the stiffener blade, fibre fracture and matrix cracking in the stiffener flange, multiple delaminations between the skin and stiffener, and matrix cracking in the skin.

significant separation between the skin and stiffener where the stiffener buckled locally away from the skin, in both the centre of the middle stiffener (stiffener 3) and close to the potting in one of the inner stiffeners (stiffener 4) on the non-loading side.

4. Comparison of results

In addition to the design calculations, an FE model with geometric imperfections was created by applying panel imperfections from the photogrammetric measurement of the unloaded panel to the V15 Nastran model. As an additional numerical comparison, the V15 Abaqus model was also analysed with a degradation methodology previously developed and implemented using the Abaqus USDFLD material user subroutine [9]. The subroutine was applied to the elements of the adhesive between the skin and stiffener, and monitored maximum stress failure criteria coupled to corresponding stiffness reductions upon satisfaction of the criteria as a means of modelling degradation in the skin–stiffener interface. The strength properties of the adhesive were taken from manufacturer data sheets [10] and are summarised in Table 5. For the USDFLD, a value of 0.1% was used as the reduction for the stiffness properties, on the basis of a parametric study and on the assumption that a value as close to zero as numerically possible was required in order to simulate the loss of load-

Table 5
Redux 312 material properties, from literature

Property	
E_1 (MPa)	3000
ν_{12}	0.30
Maximum compressive stress (MPa)	48
Maximum shear stress (MPa)	38
Maximum normal stress (MPa)	8

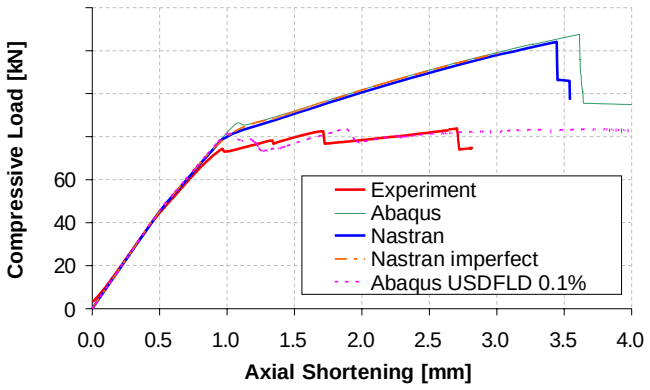

Fig. 8. Load-shortening graph, experiment versus numerical predictions.

carrying capacity by the adhesive upon failure. These computations were performed prior to the experimental testing, though were not used as part of the panel selection process, and the results using the 0.1% reduction are included only for comparative purposes. The load-shortening and deformation progression of the imperfect and USDFLD models are given in Figs. 8 and 9, respectively, which also include the Nastran and Abaqus solutions from the design analy- ses. Note that the Nastran imperfect model was only run to 3.0 mm axial compression to save computational time, which avoided the structural collapse between 3.0 and 4.0 mm compression that caused significant convergences problems and more than doubled the total computation time.

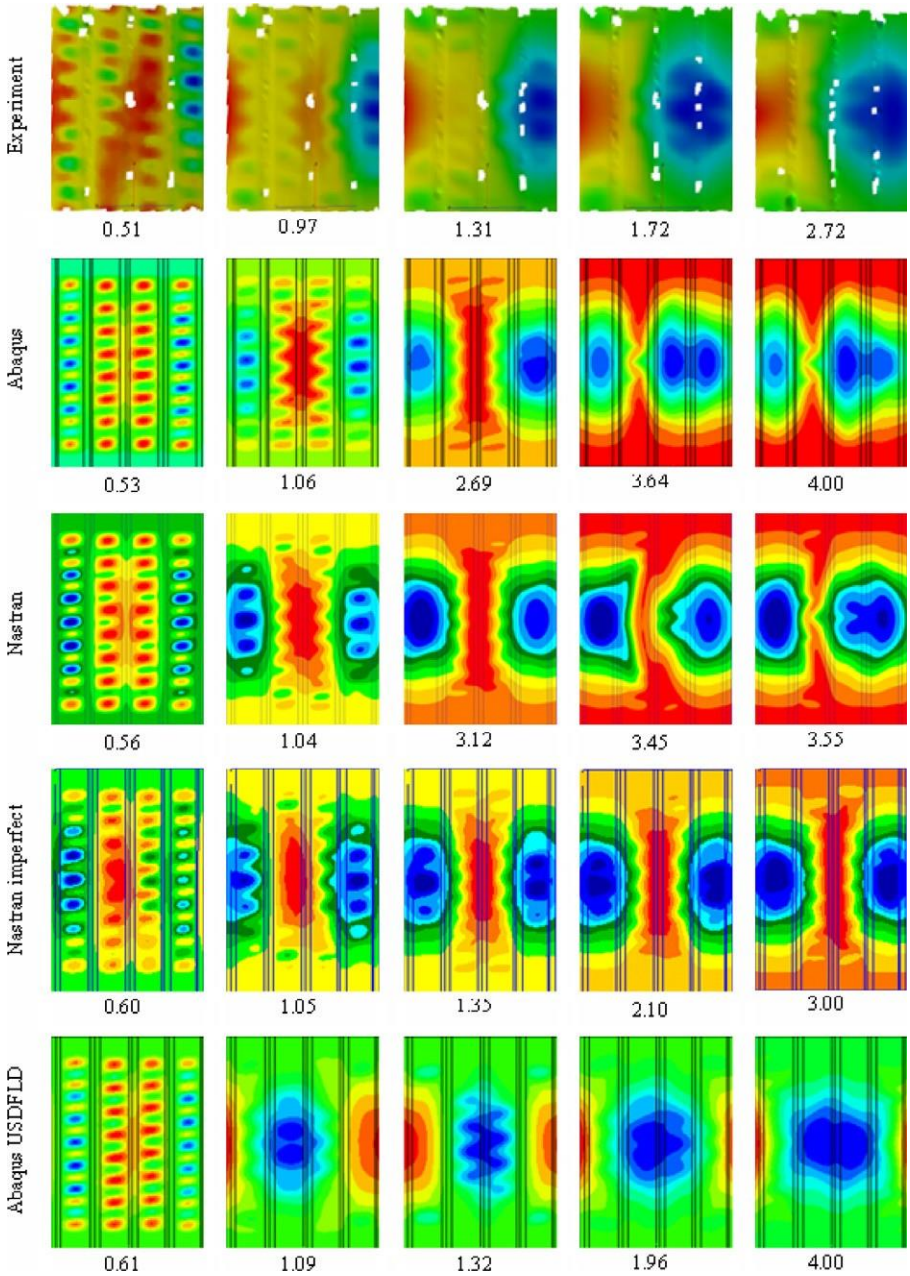

Fig. 9. Experimental and numerical deformation patterns at various values of axial compression (mm), viewed facing stiffener side.